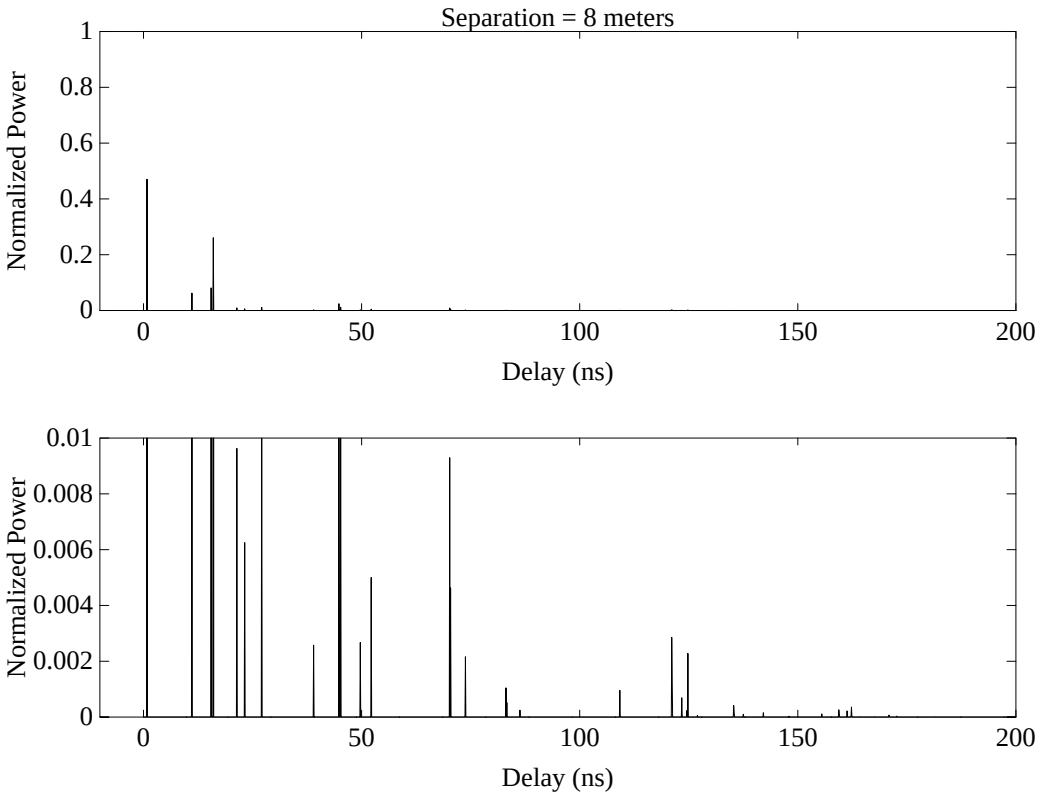

Figure 3.4: Impulse response with 8 meter transmitter/receiver separation.

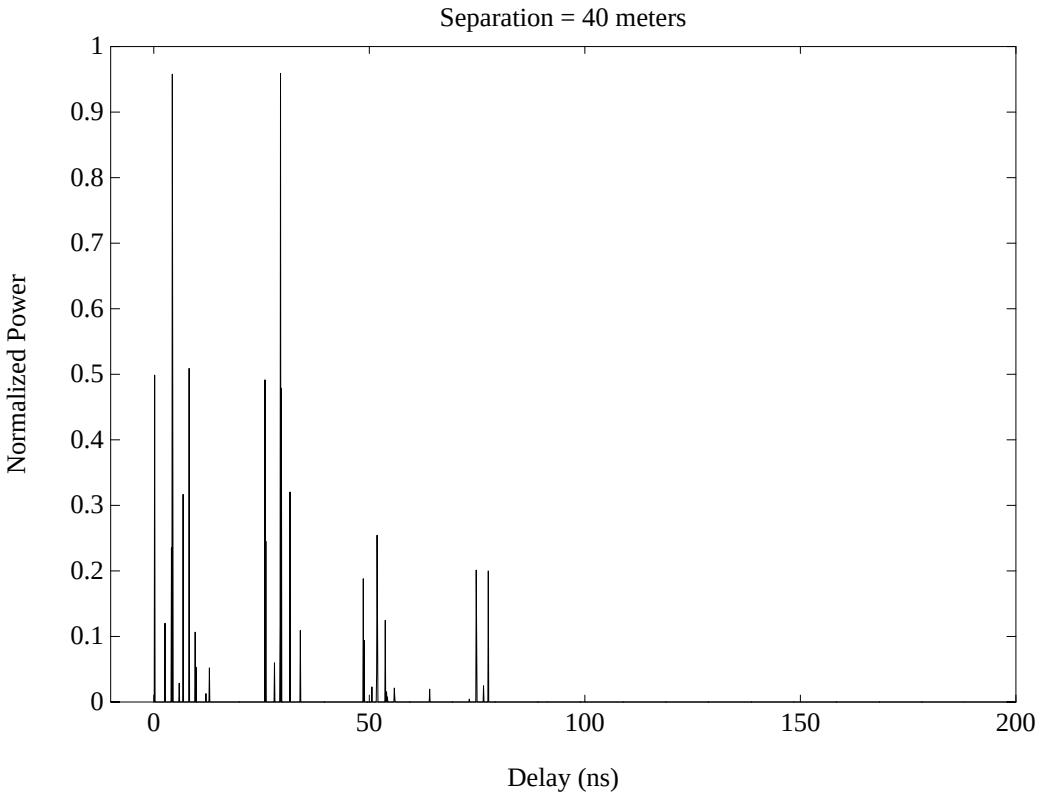

Figure 3.5: Impulse response with 40 meter transmitter/receiver separation.

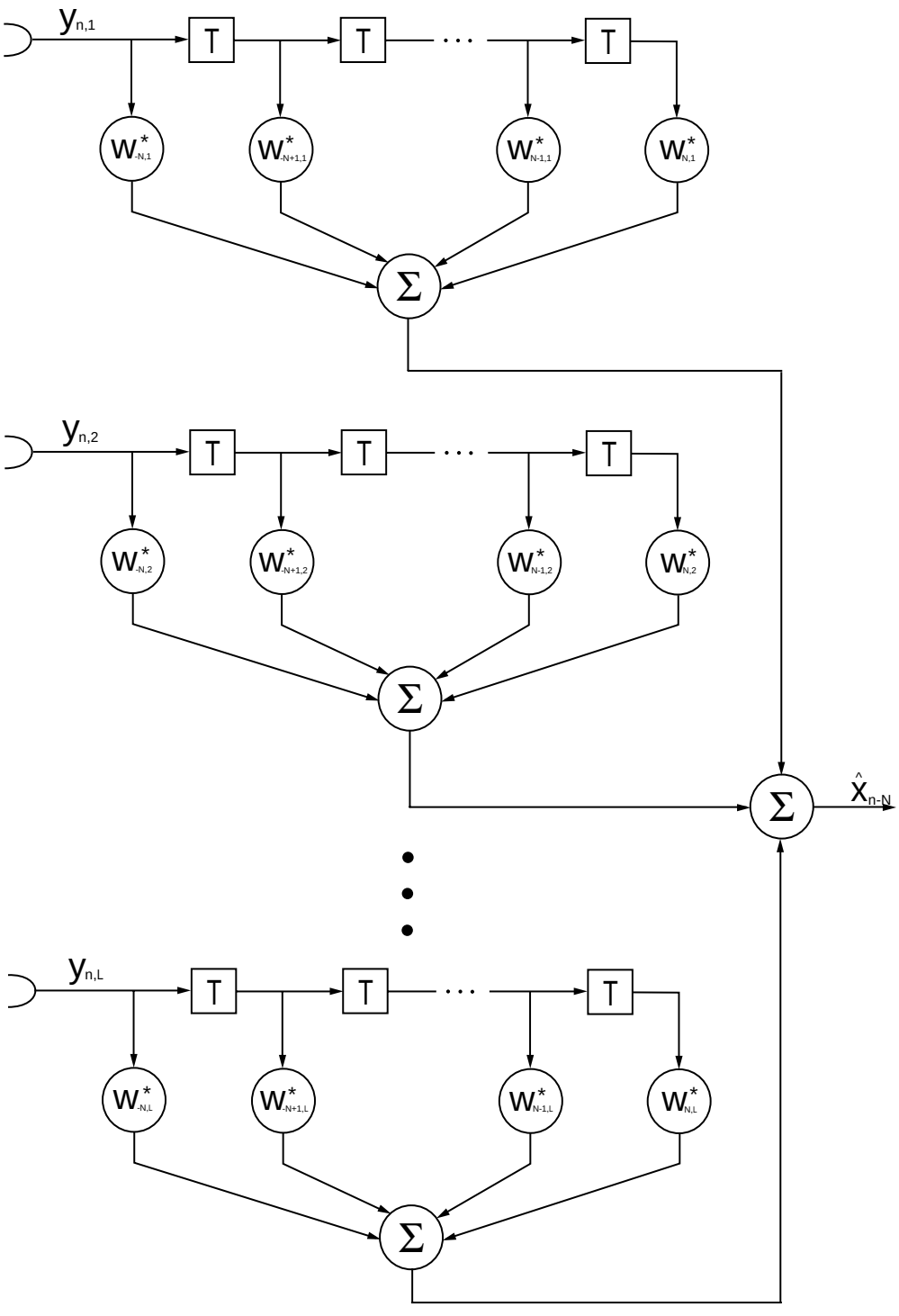

Figure 3.6: Multitap diversity combiner.

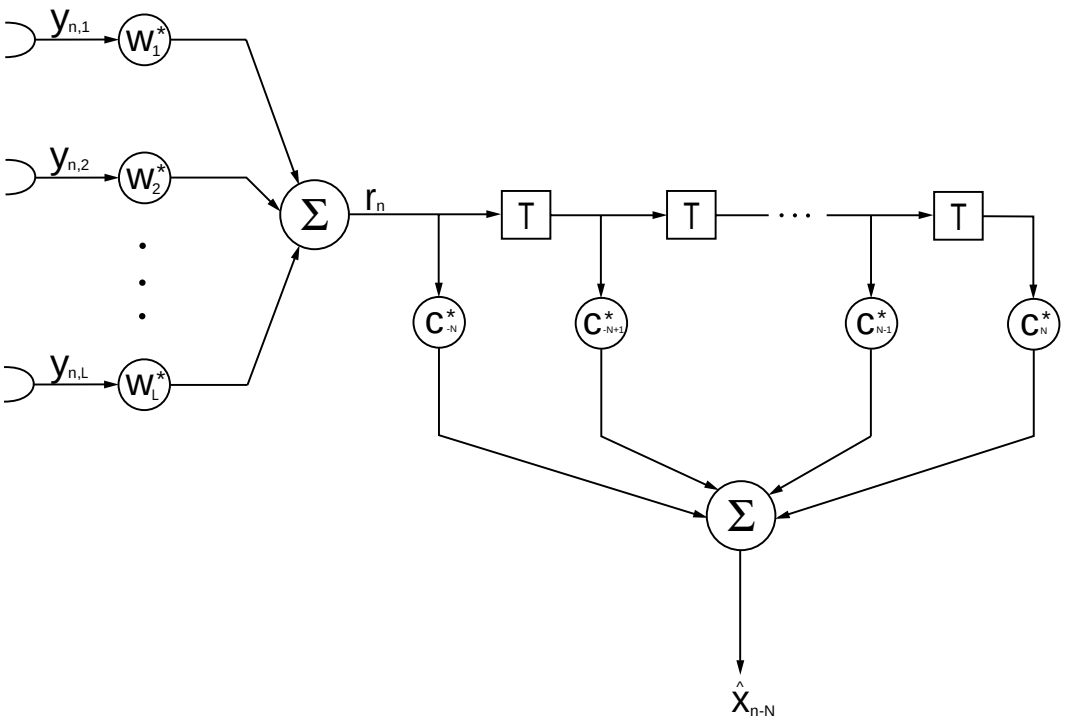

Figure 3.7: Diversity combiner followed by a linear equalizer.

In both the DC/LE and the DC/DFE, the first stage is the DC. The input from each antenna is weighted and all channels are summed. The output of the DC, r_n, is then fed into the equalizer.

The MC receiver is comprised of a LE on each antenna branch. The output of the LE for each channel is summed. The output provides an estimate of the transmitted symbol.

An equation is derived to represent the MSE between the output symbol and the transmitted symbol. We then solve for the receiver weights that minimize the MSE. In addition, we derive an upperbound for the P_e. We then evaluate the effectiveness of each receiver with these two performance measures.

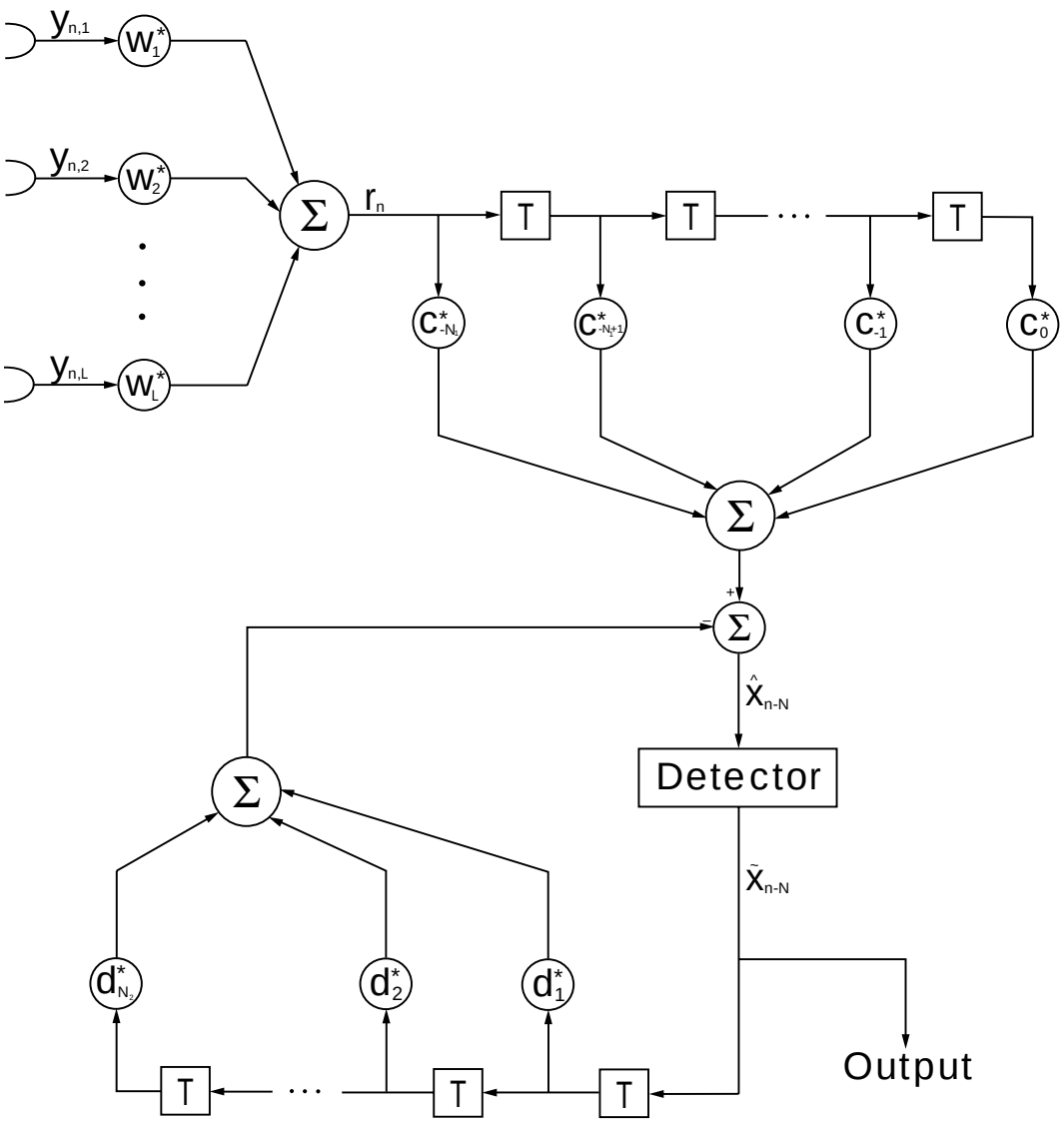

Figure 3.8: Diversity combiner followed by a decision feedback equalizer.

3.3.1 Multitap Diversity Combiner

We begin the derivation of the MSE for a system with a MC receiver with the assumption of omnidirectional transmission. Therefore the received signal is given by,

$$y_{n,k} = \sum_{i=0}^{M} x_{n-i}^{sig} h_{k,i}^{sig} + \sum_{l=1}^{I} \sum_{i=0}^{M} x_{n-i}^{int,l} h_{k,i}^{int,l} + z_{n,k} \tag{3.11}$$

where $y_{n,k}$ is the received signal at time n and antenna element k. The user transmitting the data we wish to receive is denoted by 'sig' and the interfering users are denoted by 'int'. The i^{th} of M channel taps, at the k^{th} antenna element is denoted by $h_{k,i}$.

The output of the MC with L antennas and $2N+1$ taps per antenna is given by,

$$\hat{x}_n^{sig} = \sum_{k=1}^{L} \sum_{j=-N}^{N} w_{j,k}^* y_{n-j,k} \tag{3.12}$$

The MSE is

$$\begin{aligned}
\text{MSE} &= E\left[\left|\hat{x}_n^{sig} - x_n^{sig}\right|^2\right] \qquad (3.13)\\
&= \sigma_x^2 \sum_{k=1}^{L} \sum_{m=1}^{L} \underbrace{\sum_{j=-N}^{N} \sum_{i=0}^{M} \sum_{q=-N}^{N} \sum_{p=0}^{M}}_{i+j=p+q} w_{j,k}^* w_{q,m} h_{k,i}^{sig} h_{m,p}^{sig\,*} - \\
&\quad \sigma_x^2 \sum_{k=1}^{L} \underbrace{\sum_{j=-N}^{N} \sum_{i=0}^{M}}_{i+j=0} w_{j,k}^* h_{k,i}^{sig} - \sigma_x^2 \sum_{k=1}^{L} \underbrace{\sum_{j=-N}^{N} \sum_{i=0}^{M}}_{i+j=0} w_{j,k} h_{k,i}^{sig\,*} + \sigma_x^2 + \\
&\quad \sigma_x^2 \sum_{k=1}^{L} \sum_{m=1}^{L} \underbrace{\sum_{j=-N}^{N} \sum_{i=0}^{M} \sum_{q=-N}^{N} \sum_{p=0}^{M}}_{i+j=p+q} w_{j,k}^* w_{q,m} \sum_{l=1}^{I} h_{k,i}^{int,l} h_{m,p}^{int,l*} +
\end{aligned}$$

$$\sigma_z^2 \sum_{k=1}^{L} \sum_{j=-N}^{N} w_{j,k} w_{j,k}^* \tag{3.14}$$

We expand this equation and rewrite it in vector form. We define the $(2N+1)L$ by $(2N+1)L$ matrix $\mathbf{\Phi}$ as follows.

$$\begin{aligned} \mathbf{\Phi} &= [\phi(k+L(j+N), m+L(q+N))] \qquad (3.15) \\ &= \sigma_x^2 \underbrace{\sum_{i=0}^{M} \sum_{p=0}^{M}}_{i+j=p+q} \left\{ h_{k,i}^{sig} h_{m,p}^{sig\ *} + \sum_{l=1}^{I} h_{k,i}^{int,l} h_{m,p}^{int,l*} \right\} + \end{aligned}$$

$$\begin{cases} \sigma_z^2 & k+L(j+N) = m+L(q+N) \\ 0 & \text{otherwise} \end{cases} \qquad (3.16)$$

$$k, m = 1, \cdots L \quad j, q = -N, \cdots N$$

In addition we define $\mathbf{w} = \left[w_{k+L(j+N)} \right]$ and $\mathbf{s}$ as follows. If N is less than or equal to M then $\mathbf{s}$ has the following form.

$$\mathbf{s}^T = \sigma_x^2 [\underbrace{h_{1,N}^{sig} \ \cdots \ h_{L,N}^{sig} \ h_{1,N-1}^{sig} \ \cdots h_{L,N-1}^{sig} \ \cdots \ h_{1,0}^{sig} \ \cdots \ h_{L,0}^{sig}}_{(N+1)\cdot L} \ \underbrace{0 \ \cdots \ 0}_{N \cdot L}] \tag{3.17}$$

Otherwise if N is greater than M then $\mathbf{s}$ has the following form.

$$\mathbf{s}^T =$$

$$\sigma_x^2 [\underbrace{0 \ \cdots \ 0}_{(N-M)\cdot L} \underbrace{h_{1,M}^{sig} \ \cdots \ h_{L,M} \ h_{1,N-1}^{sig} \ \cdots h_{L,N-1}^{sig} \ \cdots \ h_{1,0}^{sig} \ \cdots \ h_{L,0}^{sig}}_{(M+1)\cdot L} \ \underbrace{0 \ \cdots \ 0}_{N \cdot L}] \tag{3.18}$$

Therefore the equation for the MSE in vector form is

$$\text{MSE} = \mathbf{w}^H \mathbf{\Phi} \mathbf{w} - \mathbf{w}^H \mathbf{s} - \mathbf{s}^H \mathbf{w} + \sigma_x^2 \tag{3.19}$$

We minimize the MSE with respect to the antenna weights. We then solve for the antenna weights which are given by $\mathbf{w} = \mathbf{\Phi}^{-1}\mathbf{s}$. The MSE can be rewritten as $\sigma_x^2 - \mathbf{s}^H\mathbf{\Phi}^{-1}\mathbf{s}$.

3.3.2 Diversity Combiner Followed by an Equalizer

A single tap diversity combiner can be expressed as an MC with $N = 0$. The output of the DC is expressed as,

$$r_n = \sum_{i=0}^{M} x_{n-i}^{sig} g_i^{sig} + \sum_{l=1}^{I}\sum_{i=0}^{M} x_{n-i}^{int,l} g_i^{int,l} + \hat{z}_n \tag{3.20}$$

$$g_i^{sig} = \sum_{k=1}^{L} w_k^* h_{k,i}^{sig} \tag{3.21}$$

$$g_i^{int,l} = \sum_{k=1}^{L} w_k^* h_{k,i}^{int,l} \tag{3.22}$$

$$\hat{z}_n = \sum_{k=1}^{L} w_k^* z_{n,k} \tag{3.23}$$

The output of a $2N + 1$ tap length LE is given by,

$$\hat{x}_n^{sig} = \sum_{j=-N}^{N} c_j^* r_{n-j} \tag{3.24}$$

where c_j are the equalizer weights. The output of DFE with a feedforward filter of length $N_1 + 1$ and a feedback filter of length N_2 is given below.

$$\hat{x}_n^{sig} = \sum_{j=-N_1}^{0} c_j^* r_{n-j} - \sum_{k=1}^{N_2} d_k^* \tilde{x}_{n-k}^{sig} \tag{3.25}$$

where c_j are the feedforward filter taps and d_k are the feedback filter taps. The output of the decision decision device is given by $\tilde{x}_n^{sig}$.

Using a similar procedure to Section 3.3.1, we can find the equalizer tap weights. See Appendix B.2 for complete details.

3.3.3 Probability of Error

To avoid lengthy error probability simulations, we derive an upper bound on P_e as a function of the MSE. From Eq. 2.35, with the signal set size equal to 2^k, the expression for the probability of error is given as,

$$P_e = 1 - \left[1 - 2(1 - 2^{-k/2})p\right]^2 \tag{3.26}$$

The variable p is given in Eq. B.43 and is a function of numerous differently distributed random variables. Therefore we will find an upper bound on p, by using the Chernoff bound. See Appendix B.3 for the derivation. The final form of p is,

$$p \leq \exp\left[\frac{-\varepsilon/2}{(\text{MSE})}\right] \tag{3.27}$$

3.3.4 Simulation Results

To simulate the performance of the receivers we created a floor of an office building, divided into three cells with a pair of users randomly placed in each cell. The receivers were composed of a nine element antenna array for reception, with omnidirectional transmission. The channel from every user to every antenna element of every other user was determined, yielding the received signal and the co-channel interference. For each receiver the optimal receiver weights for the minimum MSE of the system were

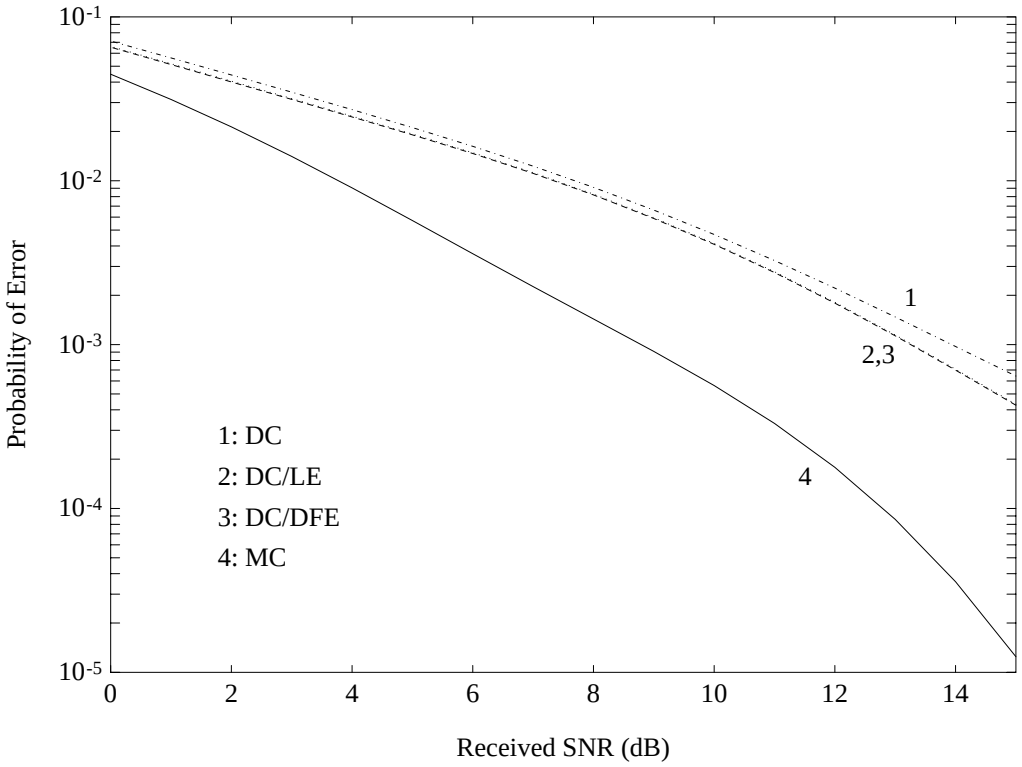

Figure 3.9: Probability of error vs. received SNR for adaptive receiver simulation.

calculated for a range of signal-to-noise ratios (SNR), based on 4-QAM modulation. The symbol rate was $16MHz$. To reduce the length of the simulation, the receiver weights were analytically calculated to determine the MSE and an upperbound on P_e. This was repeated for many different user placements to produce averaged results. The results are given in Figure 3.9.

We see from Figure 3.9 that for $P_e = 10^{-3}$, the MC yields a reduction in the required received SNR of almost $5dB$ as compared to the DC. We see that the DC/LE and DC/DFE are both less than $1dB$ better than the DC alone.

The performance of the DC with a large number of antennas limits the effectiveness of equalization. The DC reduces the ISI caused by delayed responses in the indoor radio environment by placing a null in the beampattern of the antenna array in the direction of the ISI. In addition the indoor radio environment is dominated by CCI and the ISI is minimal as compared to the mobile radio environment. Therefore the effect of an equalizer following a DC on the MSE is small. In addition, the equalizers have no effect on co-channel interference. On the other hand, with the MC, the multiple taps for each antenna branch allows for joint adaption in time and space. This results in the optimal reduction of both the ISI and CCI yielding a large performance gain.

We conclude that additional antenna elements provide much more gain than additional equalizer taps. However, the result is much more expensive hardware, since each adaptive antenna element demands either a separate downconverter path or highly linear and well-matched complex RF adaptive multipliers.

3.4 Adaptive Transmission

With an iterative algorithm the receiver weights are adaptively calculated based on minimizing the measured error. In this manner, the receiver can adapt to changes in the channel. However, on transmission there is no error information with which to adapt the antenna weights, and in a distributed system the transmitter has no

knowledge of the signaling environment.

To deal with these difficulties we have developed a new algorithm in which the DC receiver antenna weights are used for transmission. The receiver calculates the optimal antenna weights to null interfering signals and minimize the MSE. Therefore, if we use the same weights on transmission, we will be transmitting through nulls in the beampattern in the direction of the interfering users, thereby reducing co-channel interference in the system (assuming time-division duplex transmission and a slowly changing channel.) In addition, with a DC receiver, there is minimal additional hardware complexity in implementing the adaptive transmitter. For other receiver structures, it would be necessary to calculate DC receiver antenna weights for use on transmission. A significant benefit of this scheme is that no feedback is required between users.

To measure the performance of the transceivers, we use the same simulation as in Section 3.3, adding now the transmitter array. In Figure 3.10, we illustrate the optimal analytical simulation results. These are calculated by solving for the receiver weights which minimize the MSE for the given channel. Then the DC receiver weights are used for transmission. The receiver weights are then recalculated. This procedure is repeated until the MSE of the system converges to a stable solution. In the figure, the solid lines indicate omnidirectional transmission. This is used to compare to the adaptive transmitter algorithms. The dashed lines indicate using receiver weights for transmission (RW).

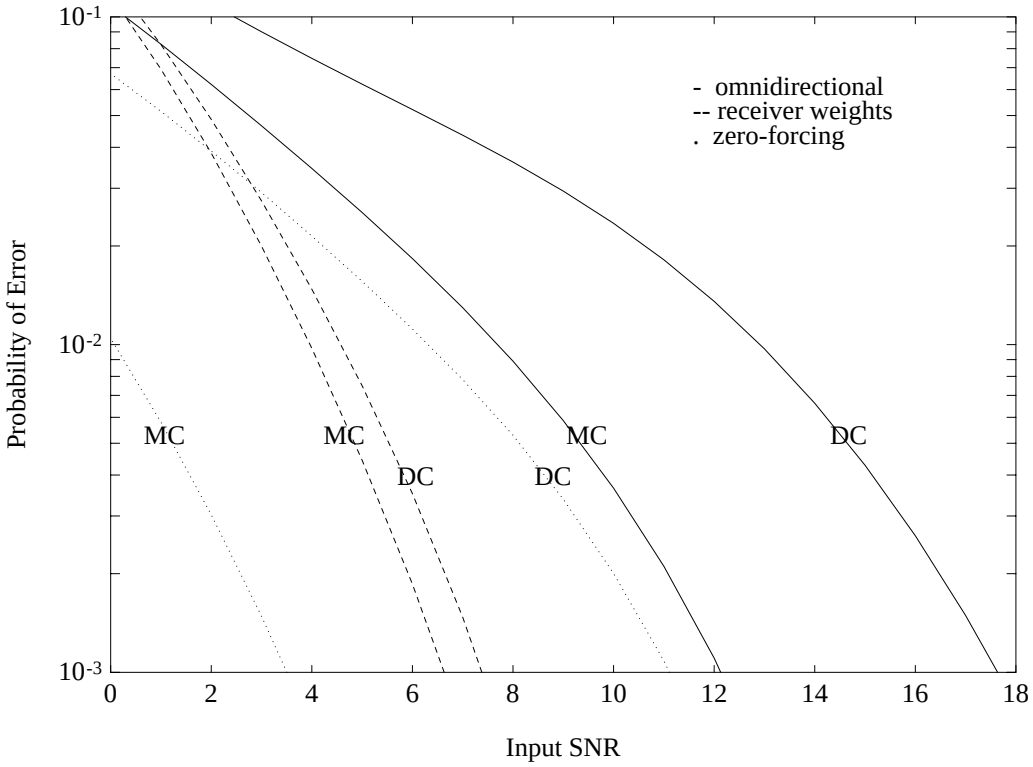

Figure 3.10: Probability of error vs. received SNR for adaptive transmitter/receiver simulation.

For comparison, we also simulated the system in which channel information between all the users in the network is fed back, with adaptation of the transmitters accomplished by a zero-forcing (ZF) solution. The derivation is given is Appendix B.4. Dotted lines in the figure indicate a ZF transmitter. For each transmitter we examine two different receivers, a single-tap diversity combiner, noted as DC in the figure, and a multitap diversity combiner with three taps per antenna, noted as MC in the figure.

As in Section 3.3, we achieve a $5dB$ gain, at a P_e of 10^{-3}, with the MC receiver

over the DC receiver, with omnidirectional transmission. Comparing the transmitter structures, we achieve the best performance with the ZF transmitter and an MC receiver. This structure yields a $3dB$ gain over the RW transmitter and an MC receiver. In addition, the ZF transmitter results in more than a $8dB$ gain over omnidirectional transmission. But this performance gain is at the cost of a tremendous increase in system and hardware complexity. On the other hand, using the RW transmitter attains a $5dB$ performance gain over omnidirectional transmission with a small increase in system and hardware complexity.

An important result is that with the RW transmitter only a $1dB$ gain is achieved by using an MC receiver instead of a DC receiver. However in Section 3.3 we saw a $5dB$ gain using the MC receiver as opposed to the DC receiver. Since the adaptive transmitter greatly reduces the CCI, the benefits of the MC receiver are now greatly diminished. Therefore, for a minimal loss in performance, we can significantly simplify our transceiver design by only implementing a DC receiver. For transmission we can then use the receiver weights directly without having to calculate a separate set of weights for the transmitter.

3.5 LMS Adaptation of the Transceiver Structure

3.5.1 General Performance

We now examine the performance of a realistic implementation of the adaptive transceiver. To analytically derive the receiver weights as discussed above requires knowledge of the channel characteristics in the form of a channel covariance matrix. This information could be provided by implementing a channel estimator. But the derivation also requires a matrix inversion of the covariance matrix. Matrix inversions are computationally costly.

An alternative approach is to iteratively adjust the weights by the steepest descent method. After the detection of every symbol we adjust the weights based on the error between the transmitted symbol and the output of the decision device. If convergence is possible, we eventually will attain the receiver weights which minimize the MSE. This is the least-mean-square (LMS) algorithm [51]. This algorithm is simple and yet capable of achieving satisfactory performance under the right conditions. It's major limitation the relatively slow rate of convergence [26]. For an indepth analysis of the LMS algorithm see [26].

We have chosen the LMS algorithm for its simple implementation due to the

hardware constraints of the system. Other iterative algorithms such recursive least-squares (RLS), which is based on Kalman filtering theory, would provide typical convergence rates of an order of magnitude faster than the LMS algorithm. This improvement in performance, however, is achieved at the expense of a large increase in computation complexity [26], which we cannot afford.

The adaptation of the transceiver is accomplished by first updating the the receiver weights. The general form of the update is,

$$\mathbf{w}_{i+1} = \mathbf{w}_i + \Delta e_i \mathbf{y}_i \tag{3.28}$$

where $\mathbf{w}_i$ denotes the vector of receiver antenna weights at the i^{th} iteration, Δ denotes a positive number small enough to ensure convergence [51], e_i denotes the error in the output of the antenna array, and $\mathbf{y}_i$ denotes the input vector to the antenna array. During training of the transceiver, e_i is calculated as the difference between the value of the transmitted symbol and the output of the array. Otherwise the error is calculated as the difference between the output of the decision device and the output of the antenna array.

Through experimentation, Δ equal to 0.01 was found to be appropriate. Larger values for Δ resulted in unstable conditions in which the update of $\mathbf{w}_i$ was too large and the system diverged. Smaller values for Δ resulted in very slow rates of convergence.

To summarize the operation of the transceiver, the input from the elements of

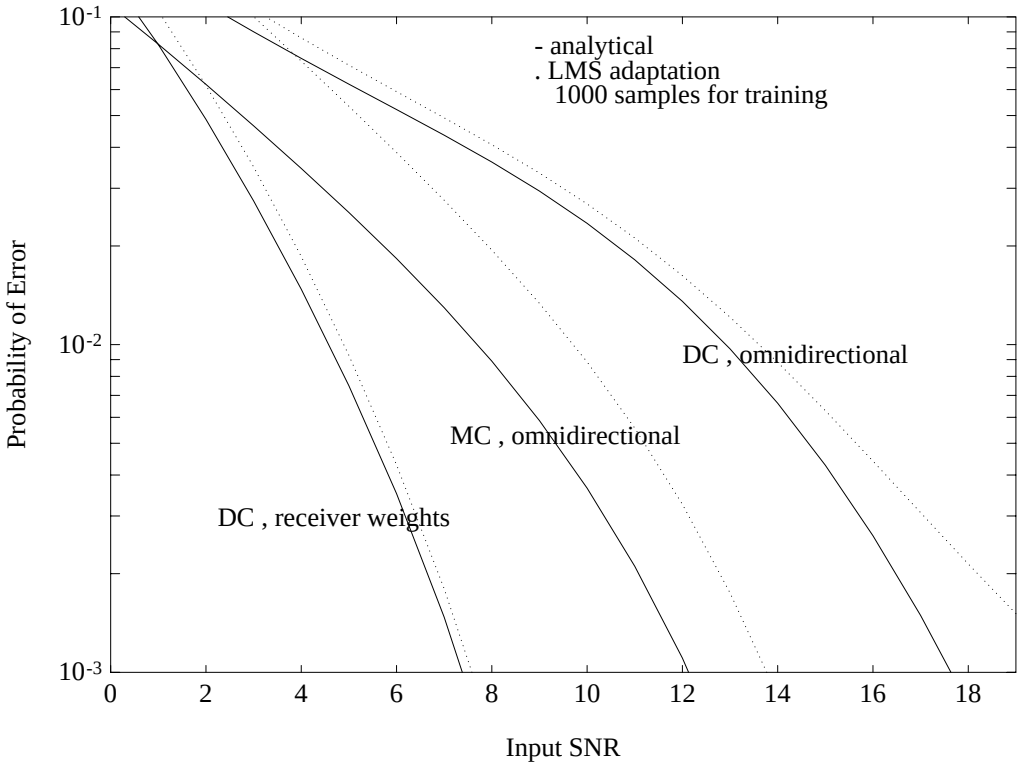

Figure 3.11: A comparison of analytical and LMS adaptive simulations.

the antenna array are multiplied by antenna weights which are then combined. The resulting output is passed through a decision device which selects the symbol which is closest in value to the output of the antenna array. This is the estimate of the transmitted symbol. Then the update of the receiver antenna weights is performed as described above. The new values of the receiver weights are also used as new transmitter weights at the next iteration.

Simulations have shown that the performance is close to optimal when allowing 1000 samples to train the transceiver, as illustrated in Figure 3.11.

3.5.2 Convergence Rates

We now examine the convergence behavior of the LMS adaptation of the transceiver. First we will explore the effects of network topology on adaptation rates. We compare the adaptation rates of a multiple cell system versus a single cell system. In the latter, the interfering users could be spaced much closer together. This illustrates the effects of the proximity of the interfering users to each other on the adaptation rates.

From simulations we found that for the multiple cell system there is almost no loss in performance with as few as 300 training symbols. The results are illustrated in Figure 3.12. For the single cell environment, the overall performance is significantly reduced, but the adaptation rate has not changed. We again found that with as few as 300 training symbols, there is little loss in performance. This is demonstrated in Figure 3.13.

However, in some cases the single cell system did not converge. When there is a strong interaction between the users in the network it sometimes occurs that when one user adapts its transmitter, all other users adapt their transmitters in reaction. This again causes a strong reaction by all the users and they all adapt again, and so forth. The network oscillates with no convergence, or diverges. In addition, there are cases where an interferer is in much closer proximity to a user than its partner. The interference strongly dominates the received signal and causes the adaptation of the transceiver to diverge.

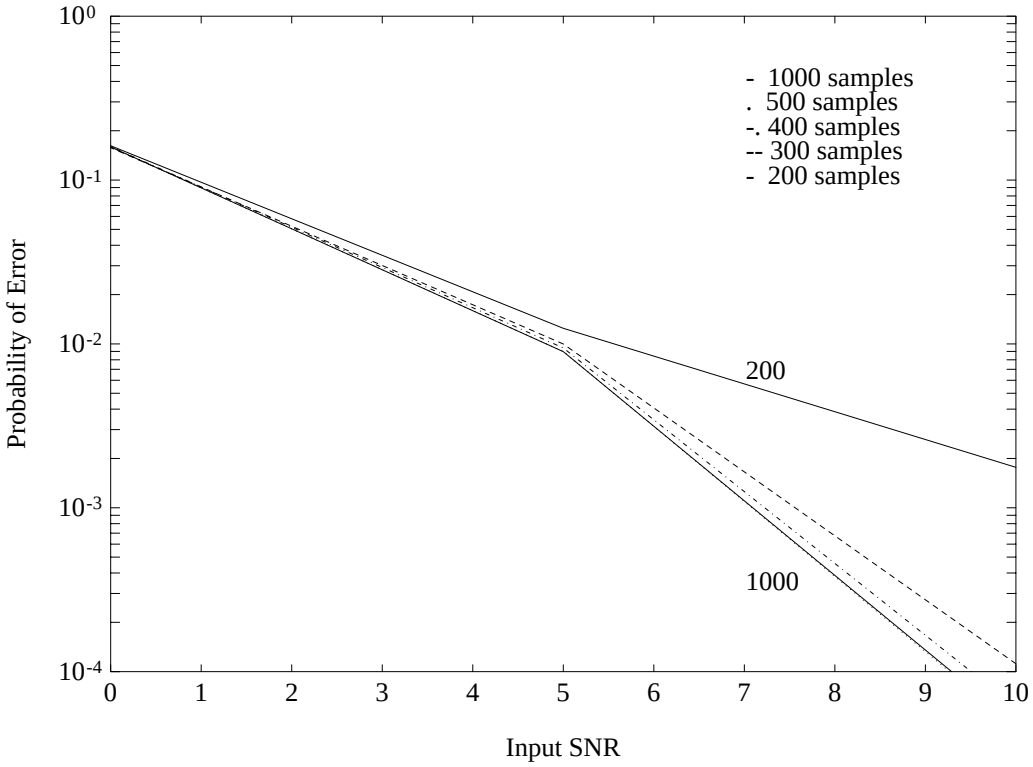

Figure 3.12: Six users, one pair per cell; DC receiver; receiver weights for transmission.

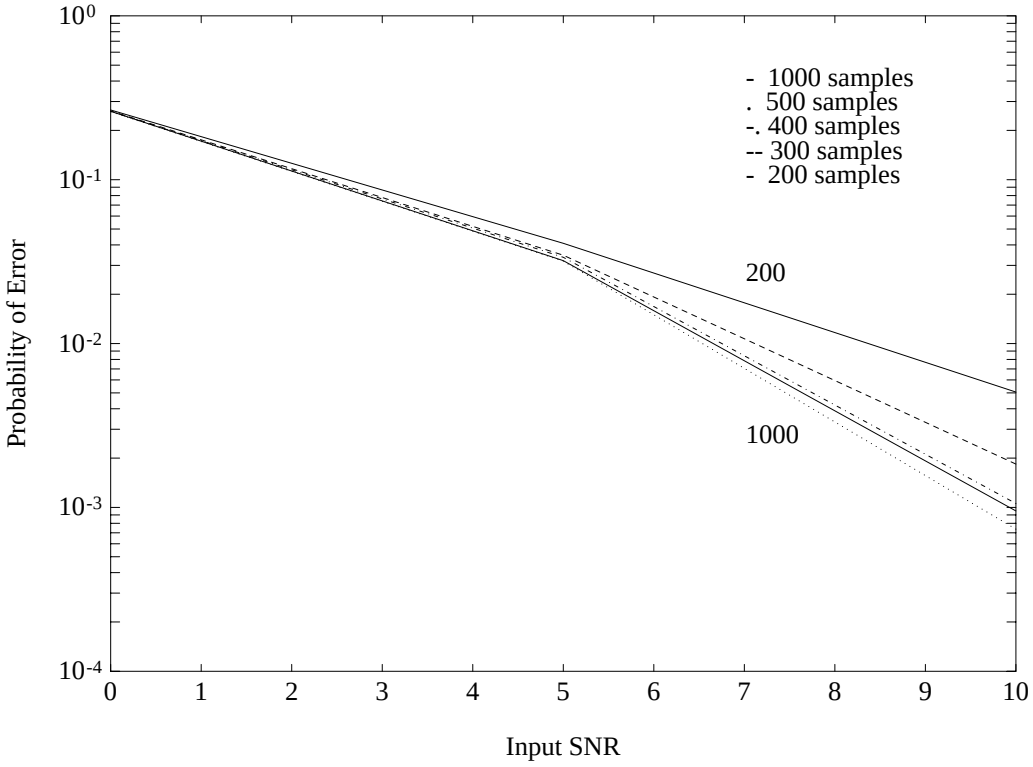

Figure 3.13: Six users in one cell; DC receiver; receiver weights for transmission.

Distributed operation requires that such events be very rare. We must ensure that the primary factor governing adaptation should be the users' own link. When we implement a multicell system with orthogonal signaling to reduce CCI, we are also decoupling the users in the network. By reducing the interaction between users we ensure system convergence. In addition, our complete system design will include line-probing and power control algorithms which will only allow users to enter the system in a high SNR environment. With these algorithms we are further ensuring that the interaction between interfering users will be limited.

We now consider two different operating scenarios. Suppose first that the users are active for only a short period of time, as for example in bursty data transmission. In addition, if we implement a frequency-hopped system, the users will also only transmit at a given frequency for a short time. These situations result in the users constantly retraining their transceivers. Therefore we may have many users entering the system and training simultaneously. We compare this system to one in which users are active for long periods of time, such as voice communication. Therefore a new user would enter a stable system.

We have simulated six users training simultaneously. As before using a training sequence length of 300 symbols results in little loss in performance. When a new pair of users enters a system where four other users have already trained and are fully adapted, 200 symbols for training suffice, as seen in Figure 3.14.

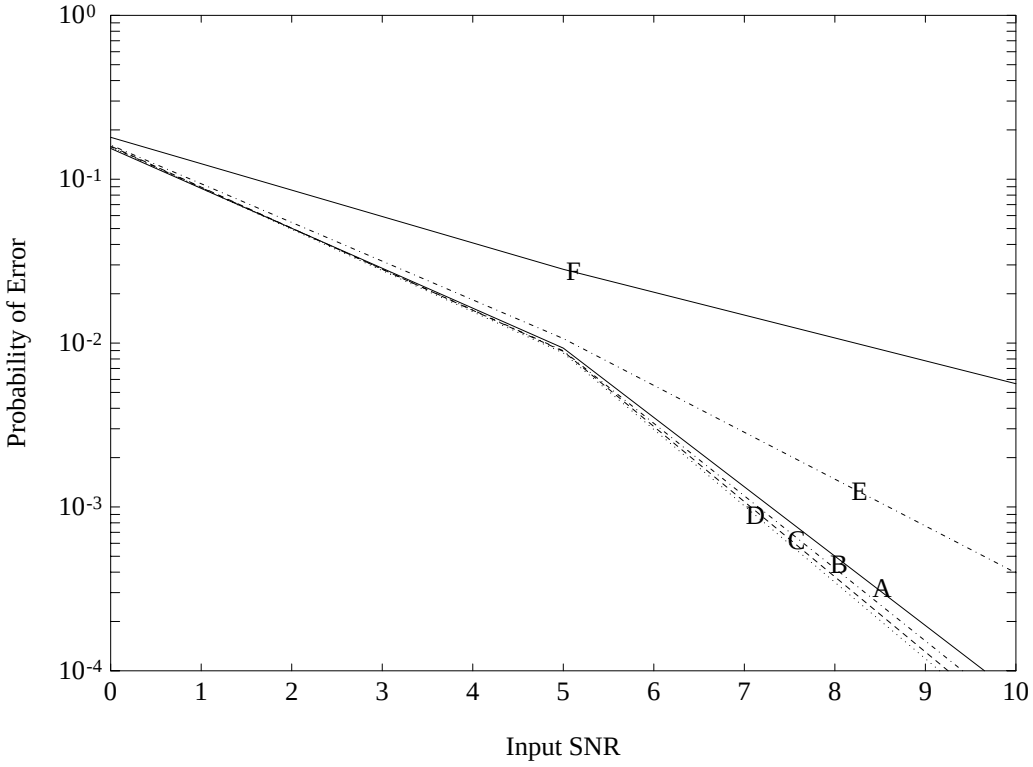

Figure 3.14: Four completely adapted users in the system, one new pair of users enters the system; one pair of users per cell; DC receiver; receiver weights for transmission. Line (A) illustrates the system performance with two pairs of users. Line (F) demonstrates the results when a new pair enters the system with omnidirectional transmission. Lines (B-D) give the results when the new pair use the receiver weights for transmission and trains the transmitter with 200, 500, and 1000 symbols, respectively. Line (E) is similar except only 100 symbols are used for training.

3.6 A More Robust System

Our simulations of the indoor environment have shown that on average small delay spreads result in little benefit from equalization. This is especially true when utilizing a large antenna array for diversity combining. In addition, we have shown that the dominant interference is CCI, which is not reduced by equalization. However, occasionally ISI will limit performance, particularly when we wish to employ large constellations.

In Figure 3.15 we illustrate the analytical results of adding an LE or a DFE following the DC. The signaling environment is comprised of significant ISI and no CCI. We still see that the DC/LE with 9 equalizer taps provides almost no gain over the DC alone. Therefore the adaptive transmitter and the DC receiver must still be able to place nulls in the beampattern in the directions of the significant ISI and also smooth out channel spectrum nulls. We do see a $1.5dB$ gain in performance at a P_e of 10^{-3} when implementing the DC/DFE with 5 feedforward taps and 4 feedback taps. However, all the performance gain is due to the feedback filter; the same system performance is achieved with no feedforward taps. The DC/DFE with 0 feedforward taps and 8 feedback taps provides a system performance gain of almost $2.5dB$ over a DC alone.

Adding the DFE may reduce the speed of adaptation. We simulate the performance of the adaptive transceiver with a DFE following the DC with 5 feedforward

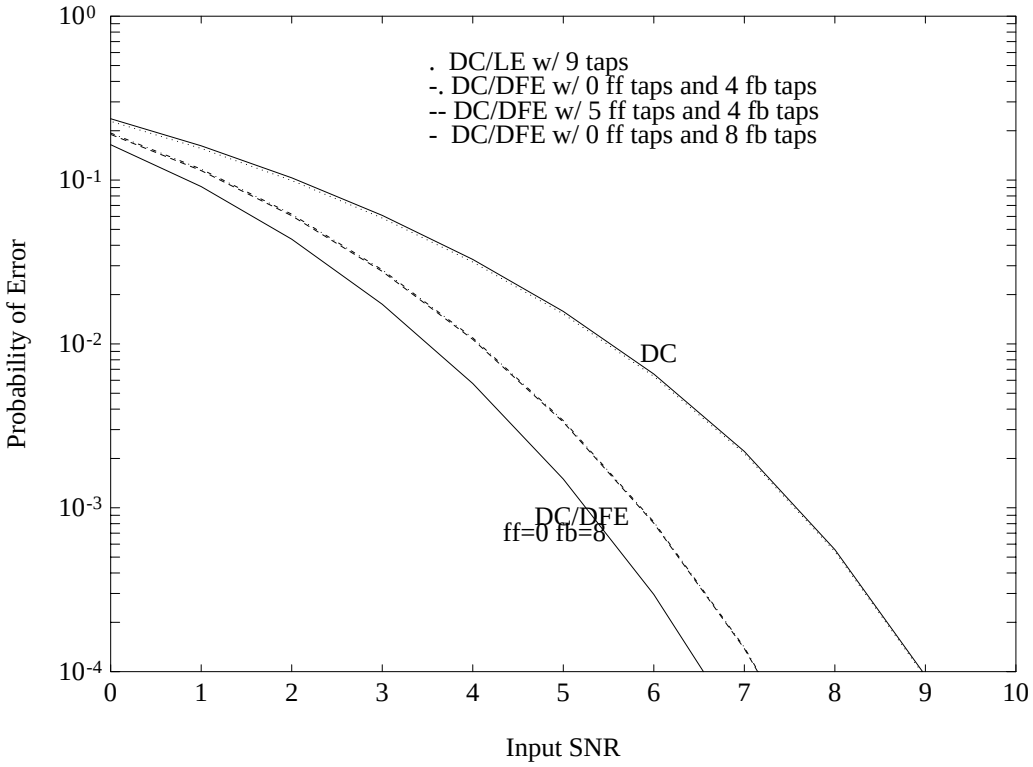

Figure 3.15: Analytical simulation results with equalization in an ISI signaling environment.

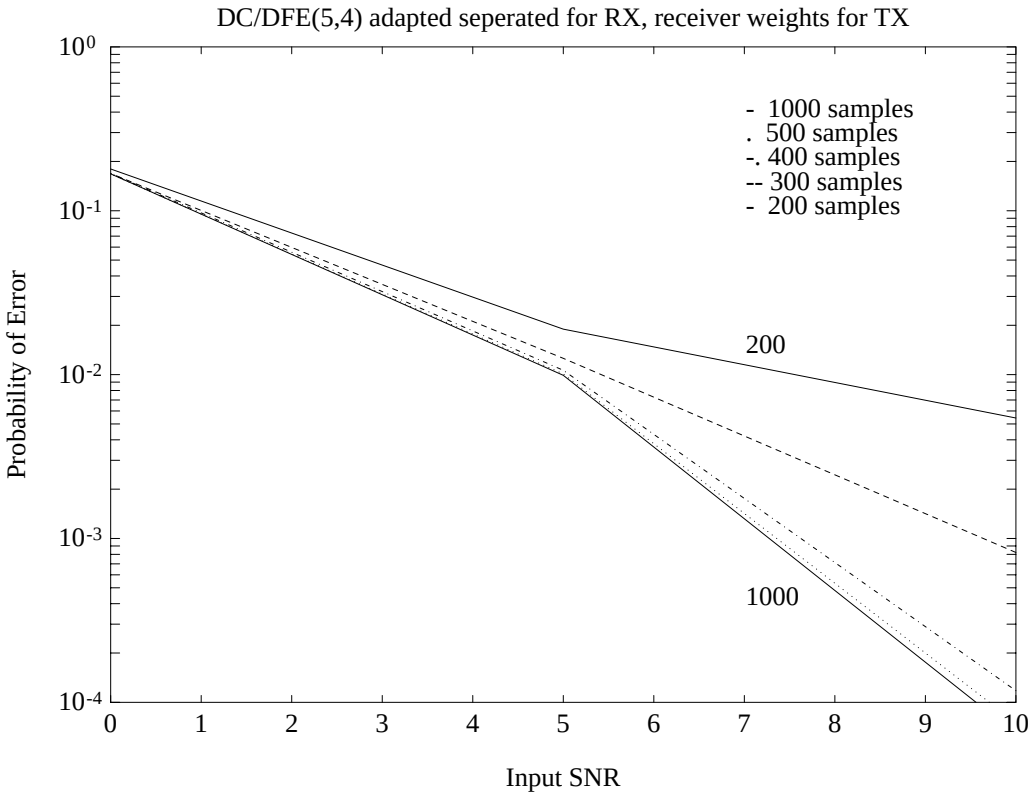

Figure 3.16: Six users, one pair per cell; DC/DFE receiver with 5 feedforward taps and 4 feedback taps; receiver antenna weights for transmission.

taps and 4 feedback taps, with a repeat of the simulation from Section 3.5.2 for a multicell system. The results are given in Figure 3.16. We now find that we require 400 training samples instead of 300 as before. We repeated the experiment with no feedforward taps and 4 feedback taps, as illustrated in Figure 3.17. For the same system performance, we see that the required number of training symbols is again reduced to 300. Greater performance was achieved in an ISI environment with no feedforward taps and 8 feedback taps. Simulations to create Figure 3.18 show that only 300 training symbols are required. Therefore a feedback filter following the

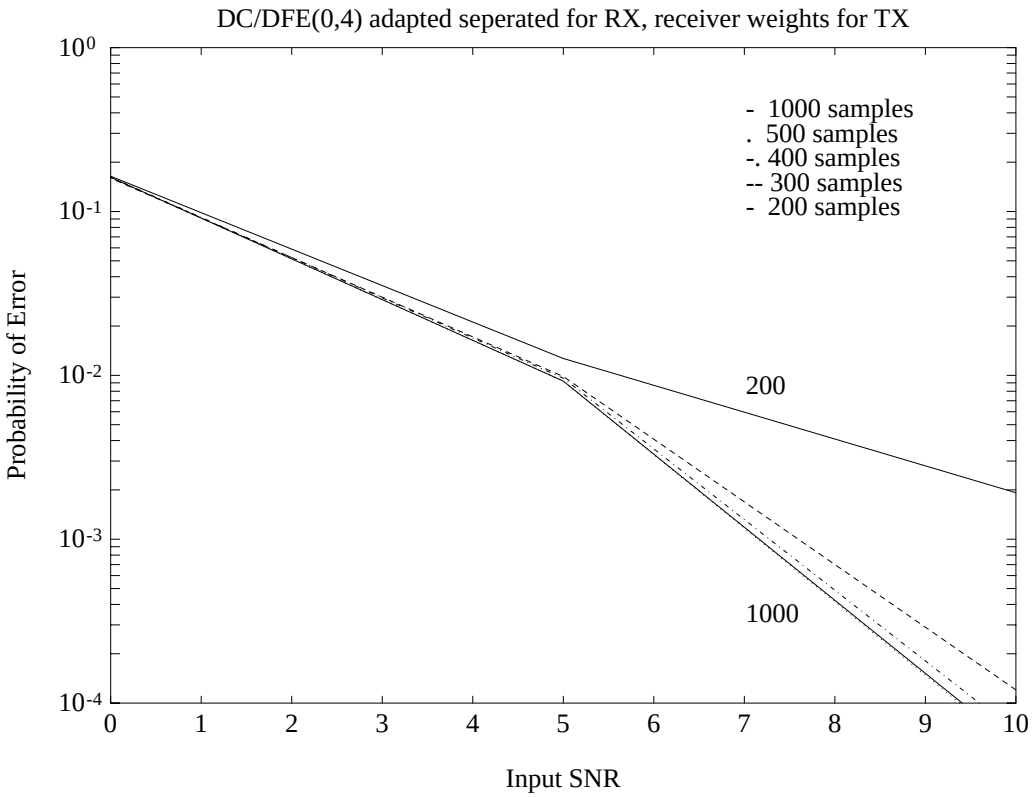

Figure 3.17: Six users, one pair per cell; DC/DFE receiver with 0 feedforward taps and 4 feedback taps; receiver antenna weights for transmission.

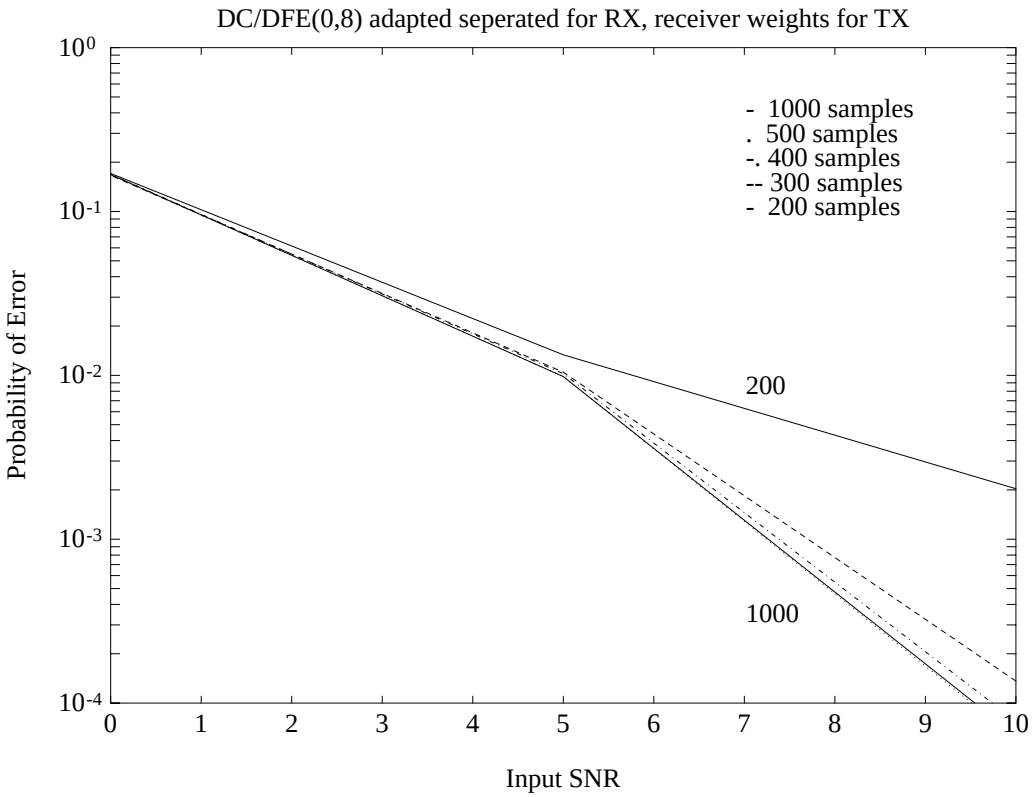

Figure 3.18: Six users, one pair per cell; DC/DFE receiver with 0 feedforward taps and 8 feedback taps; receiver antenna weights for transmission.

DC can be added with no reduction in the adaptation rate. In addition, since the feedback filter is adapted separately from the DC, we can still use the receiver DC weights for transmission.

3.7 Conclusion

In a distributed indoor system, feedback of channel information to adapt transmitters, or fixed beampatterns, is not feasible. We have developed a practical scheme of adapting the transmitters that leads to large performance gains without such interaction. The algorithm converges with mild restrictions on system coupling, using the well-known and simple LMS algorithm. The functionality of the LMS algorithm in the system design is fortunate since it significantly reduces hardware complexity.

To ensure robust performance in ISI, we include a short feedback section of the DFE after the DC for reception. We adapt the DC and the DFE separately, so as to not reduce the rate of convergence. In addition, separate adaptation of the DC and the DFE allows the DC weights to be reused for transmission, minimizing hardware complexity.

Chapter 4

Joint Adaptation of Adaptive Antennas and Power Control

4.1 Introduction

Due to limited bandwidth, cellular systems reuse frequency channels among cells. Frequency reuse is the dominant cause of CCI. If the power transmitted to a receiver is limited to the minimum level required for a quality link, interference levels at other receivers will be reduced. Therefore, in addition to the transmitter and receiver arrays, a power control algorithm will play a crucial role in reducing CCI in the system. However, a communication link becomes more vulnerable to interference when the transmitted power is reduced [87].

A power control algorithm has been incorporated in the communication system in

which users minimize their transmitting power level such that the intended receivers achieve a SINR threshold level required for adequate performance. We formulate the problem by first explicitly defining the SINR.

$$\text{SINR} = \frac{\text{Gain from transmitting to receiving partner}}{\text{CCI + ISI + AWGN}} \tag{4.1}$$

A threshold is set such that the SINR at a receiver is above a level γ. The definition for the SINR can be rewritten in terms of channel gains and transmitter power levels.

$$\begin{aligned} \text{Gain from transmitting to receiving partner} &= P_t G_{i,t}^{\text{NISI}} && (4.2) \\ \text{CCI} &= \sum_{\substack{j \neq i \\ j \neq t}} P_j G_{i,j} && (4.3) \\ \text{ISI} &= P_t G_{i,t}^{\text{ISI}} && (4.4) \end{aligned}$$

where $G_{i,t}^{\text{NISI}}$ is the gain between the i^{th} receiving user and its transmitting partner, with no ISI included. The gain due to the ISI is given as $G_{i,t}^{\text{ISI}}$. The gain between the interfering users j and the receiver user i is given as $G_{i,j}$. The transmitting power level of the partner of receiving user i is P_t, and the power level of user j is P_j. The SINR threshold of receiving user i is given by γ_i. The total number of users in the system is denoted by S. Therefore for the i^{th} receiver,

$$\frac{P_t G_{i,t}^{\text{NISI}}}{\sum_{\substack{j \neq i \\ j \neq t}} P_j G_{i,j} + P_t G_{i,t}^{\text{ISI}} + n_i} = \gamma_i \tag{4.5}$$
$$i = 1 \ldots S$$

where the AWGN at the i^{th} receiving user is denoted as n_i. A power control system

model is illustrated in Figure 4.1.

This set of equations is then solved for the transmitter power levels. In this manner, if a solution exists, all users maintain a high-quality communication link with the minimum required power. Minimizing the transmitted power reduces CCI in the system.

The power control algorithm must be adaptive to conform to slow changes in the channel. Hence, both the transceiver and power control algorithm will be adaptive. We must ensure that the joint adaptation of the adaptive antenna and the power control algorithms is feasible. Therefore, power control is included in the simulation of the LMS adaptation of the antenna weights. For ease of simulation, a centralized form of the power control will be implemented. The power control is calculated by solving the system of linear equations involving the channel gain matrix and power vector. See Appendix C for details. While several distributed algorithms exist, we anticipate that the power control algorithm actually implemented will be based on [13].

4.2 Joint Adaptation

Our first attempt was to allow the antennas to adapt for 500 iterations and then calculate the power required to achieve the SINR threshold. We observed large jumps in the SINR and the MSE and the power level after calculation of the power values.

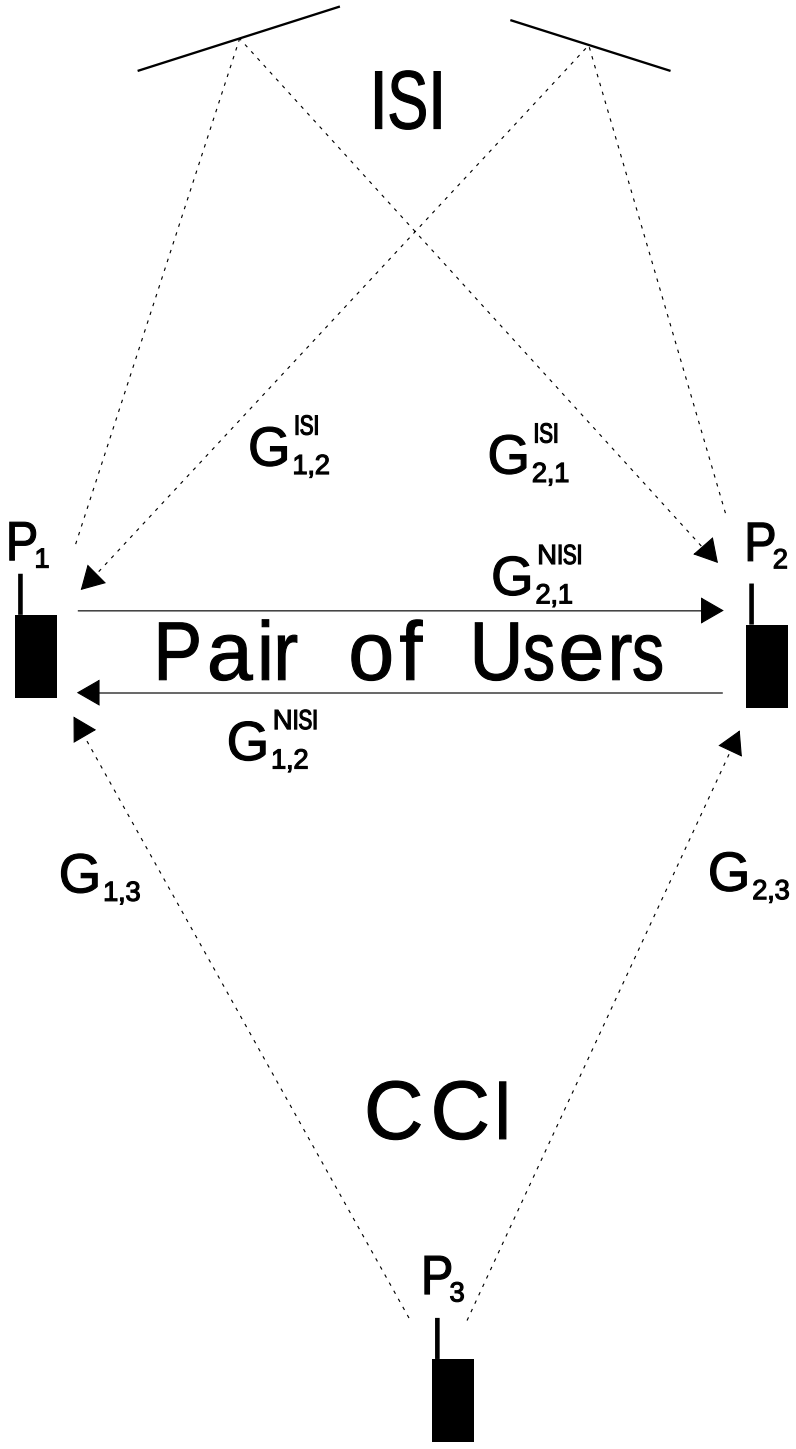

Figure 4.1: Power control system model.

The adaptive antennas were minimizing the MSE, in which case some users could be well above the SINR threshold and some could be well below. The power control forced all users to the same SINR threshold. To allow the two different algorithms to converge, many more cycles were simulated.

We observed that with each cycle the MSE, SINR, and power level would oscillate. In many cases the power level would change by large jumps after calculation of the power control vector. The large change in power would cause extremely large error vectors in the LMS adaptation of the antenna weights. In most cases the simulation diverged if enough cycles were permitted.

Three corrections were implemented in order to allow for the joint adaptation of the two algorithms. First, the allowable change in the power by the power control algorithm was limited to $1dB$ at each update. This ensured that the antenna adaptation would not be overwhelmed by the power control. Second, the power control values were recalculated every 10 iterations instead of every 500 iterations. Together this mimics a distributed, iterative implementation of the power control as in [13]. In addition, the power control now iterates to a solution on a similar time scale as the adaptive antennas.

However, the most significant change was to normalize the weights of the transmitter array. Before, both the transmitter array and the power control algorithm could cause large changes to the power level of the users. This situation created the oscillations in the simulation. By normalizing the transmitter weights such that

the main lobe of the beampattern has unity gain, the power control algorithm has full control of the power level of the users in the system. Then the sole task of the transmitter array is to minimize the interference by shaping the beampattern.

With these changes, the simulation became stable and adapted quickly.

4.3 Simulations

We now examine the performance of the joint adaptation of the antenna arrays and the power control for an example of three pairs of users at random positions and orientations. In Figures 4.2 and 4.3 we illustrate the power and SINR levels as a function of the iteration number. The initial power level is set such that the gain between each pair at the best antenna will correspond to an SNR of $0dB$ (no ISI or CCI). From Figure 4.3, we see that within 200 iterations the SINR of all users achieves the threshold of $20dB$. The system requires 200 iterations to achieve the necessary power at increments of $1dB$ with an update every 10 iterations.

However, we see from Figure 4.2 that power levels of the users had originally risen to a level above what is necessary to achieve the threshold. After 200 iterations the rate of increase of the power level greatly decreases. Therefore the antenna weights reduce the interference and the required power level is consequently reduced.

If we repeat this experiment with an initial power level corresponding to an SNR of $20dB$, we require far fewer power level steps to achieve the SINR threshold.

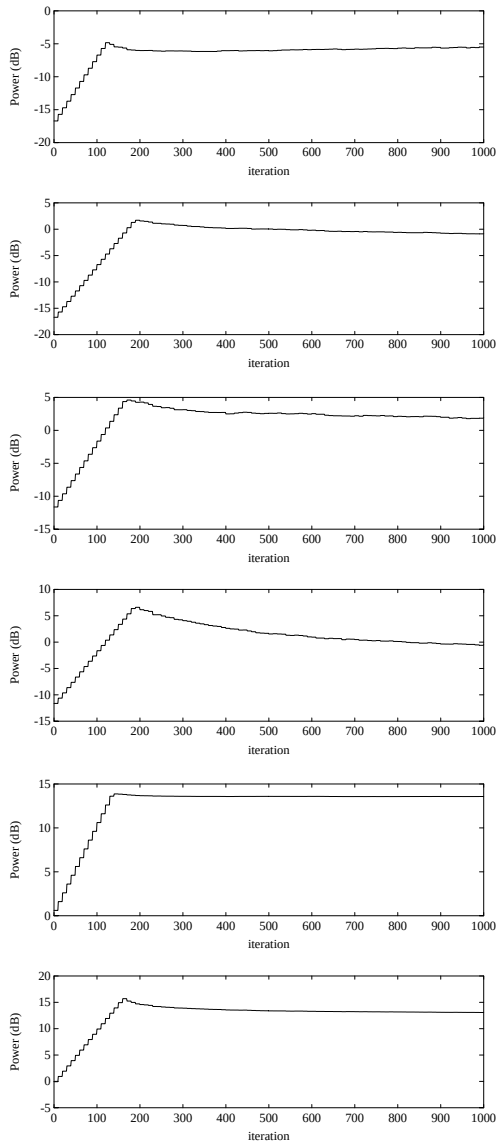

Figure 4.2: Illustration of power usage for the 6 users in the system. Initial power level based upon 0dB SNR. Receiver weights used for transmission.

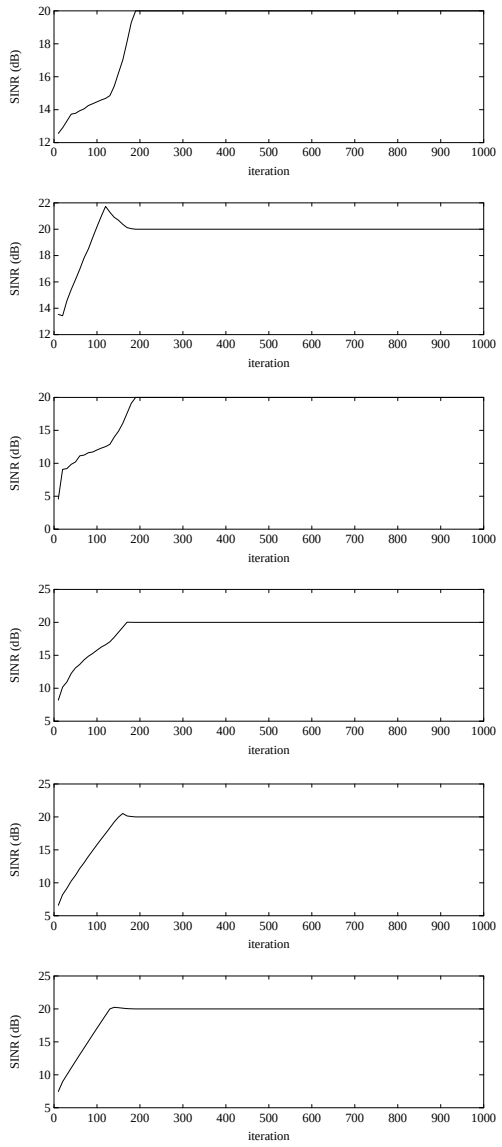

Figure 4.3: Illustration of SINR of the 6 users in the system. Initial power level based upon 0dB SNR. Receiver weights used for transmission.

Therefore the system converges more rapidly. These results are given in Figures 4.4 and 4.5. However, when a new pair of users enters the system with a high initial power level, the users already in the system will experience a large increase in the interference level. The integrity of the links of the users already in the system might be compromised. These results give an indication of the future research necessary to achieve fast adaptation of new users, while protecting the quality of the links of the old users. This will entail an in-depth investigation of distributed power control and line probing algorithms.

The final test is to ensure that the adaptive transmitter array still provides gain over an omnidirectional transmitter with the inclusion of the power control. For generalized results, this experiment has been repeated for 25 different cases. The users achieved the SINR threshold in only eight cases with omnidirectional transmission. On the other hand, the SINR threshold was achieved in 22 cases with adaptive transmission. In addition, when the users in the system achieved the SINR threshold, the system with adaptive transmission required on average a $13dB$ lower power level than the system with omnidirectional transmission. This again illustrates the dramatic performance increase achievable with adaptive transmission using receiver weights for transmission, due to the significant reduction in the interference.

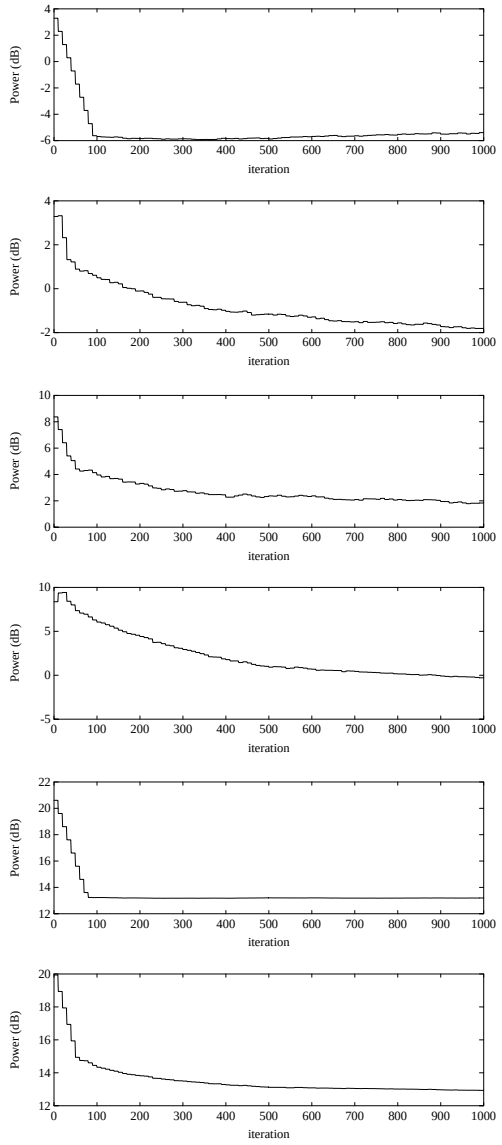

Figure 4.4: Illustration of power usage for the 6 users in the system. Initial power level based upon 20dB SNR. Receiver weights used for transmission.

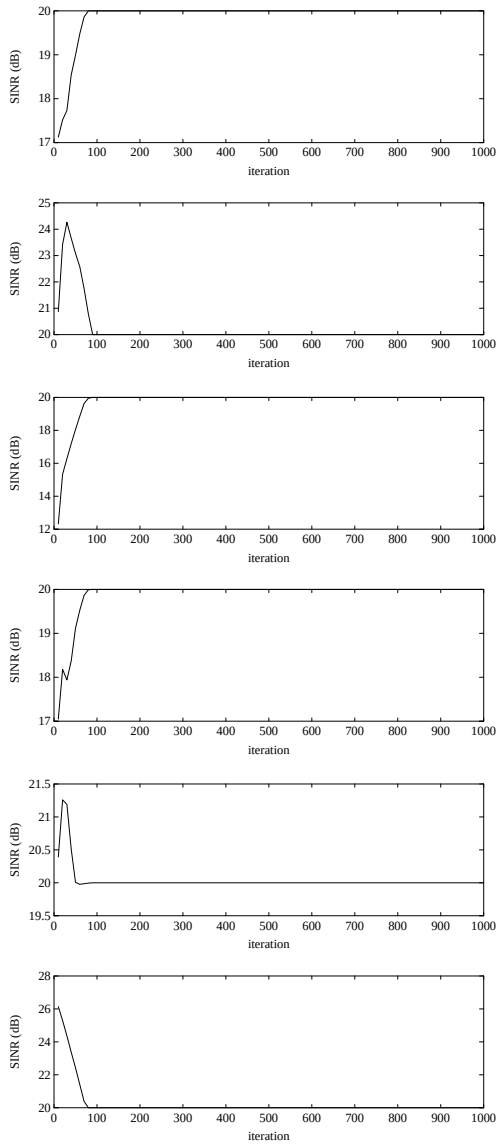

Figure 4.5: Illustration of SINR of the 6 users in the system. Initial power level based upon 20dB SNR. Receiver weights used for transmission.

4.4 Conclusion

In this chapter we have demonstrated a fundamental result that ensures the feasibility of the system design. Joint distributed adaptation of the power control algorithm and antenna arrays is stable. In addition, large performance gains over omnidirectional transmission results in large capacity increases.

Chapter 5

Conclusion

We began this research with an analytical investigation of the advantages of diversity combining in flat-fading correlated channels. With closed form solutions for the probability of error problems for many coherent and non-coherent modulation schemes, we avoided lengthy simulations that would have been necessary for testing different system designs. Even though the emphasis has been on spatial diversity in the form of antenna arrays, these results are generalized for arbitrary diversity such as coding. We have found that for all modulation schemes, large diversity gain with little loss in performance is still achieved with relatively large channel correlation. This alleviates hardware design constraints of the antenna arrays regarding coupling and correlation of the elements. Therefore we can proceed with the next project disregarding channel correlation. This greatly simplifies analytical analysis and system simulations.

In the second major research problem, the channel environment was expanded to include frequency-selective fading due to multipath and ISI. In addition, the interference was presumed to be due to competing users in the system as well as noise. This opens the possibility of gains from antenna arrays even larger than those available from diversity combining.

Our goal has been to design and demonstrate the feasibility of an adaptive, high-speed communication system. To create a high capacity system, many adaptive algorithms are implemented to reduce interference. These include adaptive antenna arrays for directional transmission, adaptive antenna arrays for beamforming on reception, adaptive equalization, and power control. With peer-to-peer communication, all adaptive algorithms must be distributed and the system be stable. We have shown that by decoupling the interaction of the interfering users in the system, stable convergence of the transceivers is ensured. In worse ISI conditions, we found that including the feedback filter of a DFE after the antenna array resulted in significant performance gains without reducing the adaptation rate of the transceiver. In addition, we found that by decoupling the adaptation of the transmitter array and the power control algorithm results in stable joint adaptation.

Further research will involve the implementation details of the adaptive transceiver. We need to establish the parameters for training the adaptive algorithms. Future research must also include developing a channel probing algorithm, to answer the following questions. What is the best method to bring in new users into a system

and not disrupt users already in the system? How does a new user quickly determine channel characteristics in a distributed system? An efficient channel probing algorithm will further limit destructive interaction between users adding to the stability of the communication system.

Appendix A

Appendix for Correlated Slowly Flat-Fading Rayleigh Channels

A.1 Appendix for PSK: Derivation of P_e for all M

The equation for P_e is given in Eq. 2.5, while $P_e(\gamma)$ and $p(\gamma)$ are given in Eqs. 2.2,2.3, and 2.18. We first derive P_e for $M = 2$ using Eq. 2.2. Substituting Eqs. 2.2 and 2.18 into the equation for P_e,

$$\begin{aligned} P_e &= \frac{(1+(L-1)\rho)^{L-2}}{2\overline{\gamma_c}(L\rho)^{L-1}} \int_0^\infty e^{-\frac{\gamma}{\overline{\gamma_c}(1+(L-1)\rho)}} \mathrm{erfc}(\sqrt{\gamma})\, d\gamma - \\ &\quad \sum_{i=0}^{L-2} \frac{(1+(L-1)\rho)^{L-2-i}}{2\cdot(L\rho)^{L-1-i}\cdot(\overline{\gamma_c})^{i+1}\cdot(1-\rho)^i\cdot i!} \int_0^\infty \gamma^i e^{-\frac{\gamma}{\overline{\gamma_c}(1-\rho)}} \mathrm{erfc}(\sqrt{\gamma})\, d\gamma \quad \text{(A.1)} \end{aligned}$$

From [51],

$$\int_0^\infty x^i e^{-x/a} \mathrm{erfc}(\sqrt{\gamma})\, dx = 2\, i!\, a^{i+1} \left(\frac{1-\mu}{2}\right)^{i+1} \sum_{k=0}^{i} \binom{i+k}{k} \left(\frac{1+\mu}{2}\right)^k \quad \text{(A.2)}$$

$$\text{where } \mu = \sqrt{\frac{a}{1+a}}$$

therefore

$$P_e = \frac{(1+(L-1)\rho)^{L-2}}{2\overline{\gamma_c}(L\rho)^{L-1}}\, 2\, a_1 \left(\frac{1-\mu_1}{2}\right) - \sum_{i=0}^{L-2} \frac{(1+(L-1)\rho)^{L-2-i}}{2 \cdot (L\rho)^{L-1-i} \cdot (\overline{\gamma_c})^{i+1} \cdot (1-\rho)^i \cdot i!} \cdot$$

$$2\, i!\, a_2^{i+1} \left(\frac{1-\mu_2}{2}\right)^{i+1} \sum_{k=0}^{i} \binom{i+k}{k} \left(\frac{1+\mu_2}{2}\right)^k \quad \text{(A.3)}$$

where $a_1 = \overline{\gamma_c}(1+(L-1)\rho)$ $\mu_1 = \sqrt{\frac{a_1}{1+a_1}}$

$a_2 = \overline{\gamma_c}(1-\rho)$ $\mu_2 = \sqrt{\frac{a_2}{1+a_2}}$

Substitution of the above variables results in Eq. 2.20.

Now we will derive P_e for $M \geq 4$ using Eq. 2.2. Substitute Eqs. 2.3 and 2.18 into Eq. 2.5 to obtain

$$P_e \approx \frac{(1+(L-1)\rho)^{L-2}}{\overline{\gamma_c}(L\rho)^{L-1}} \int_0^\infty e^{-\frac{\gamma}{\overline{\gamma_c}(1+(L-1)\rho)}} \mathrm{erfc}\left(\sqrt{\gamma}\sin\left(\frac{\pi}{M}\right)\right) d\gamma - \quad \text{(A.4)}$$

$$\sum_{i=0}^{L-2} \frac{(1+(L-1)\rho)^{L-2-i}}{(L\rho)^{L-1-i} \cdot (\overline{\gamma_c})^{i+1} \cdot (1-\rho)^i \cdot i!} \int_0^\infty \gamma^i e^{-\frac{\gamma}{\overline{\gamma_c}(1-\rho)}} \mathrm{erfc}\left(\sqrt{\gamma}\sin\left(\frac{\pi}{M}\right)\right) d\gamma$$

We use a change of variable to put the integrals in Eq. A.5 into the form of Eq. A.2. This produces Eq. 2.21 as a final result for P_e for $M \geq 4$.

A.2 Appendix for QAM

A.2.1 Derivation of P_e for Square Constellations

We begin with 16-QAM as an example. The standard constellation is a 4 by 4 grid.

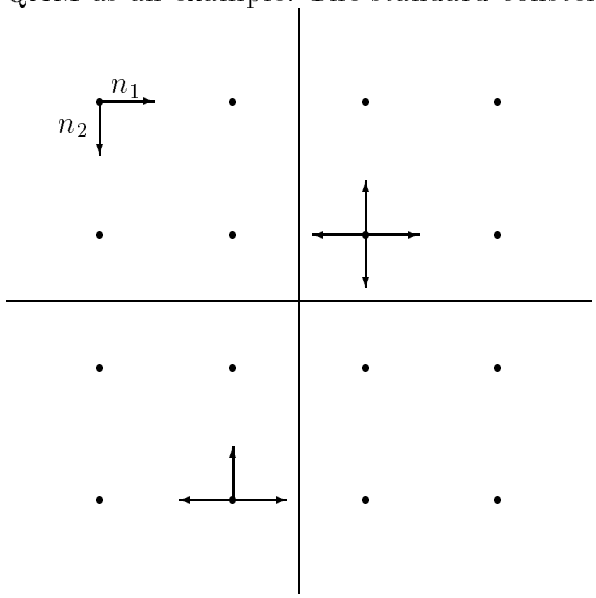

We define the minimum distance between two points as 'd'. A correct decision can be made about a received signal if the magnitude of the noise is less than $\frac{d}{2}$.

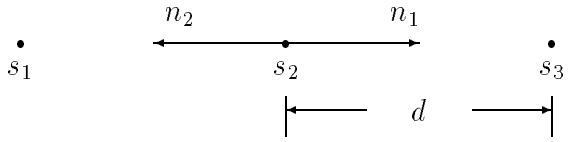

Therefore the probability of an erroneous decision is the probability that $n > \frac{d}{2}$. We define

$$p = Prob\left\{n > \frac{d}{2}\right\} \quad \text{(A.5)}$$

$$= Prob\left\{n < -\frac{d}{2}\right\} \quad \text{(A.6)}$$

We divide the signals in the constellation into three groups. The first group are the signals with two neighbors. The probability of a correct decision is expressed as

$$p_2 = Prob\left\{n_1 < \frac{d}{2}\right\} Prob\left\{n_2 > -\frac{d}{2}\right\} \quad (A.7)$$

$$= (1-p)^2 \quad (A.8)$$

The second group is the set of signals with three neighbors.

$$p_3 = Prob\left\{n_1 < \frac{d}{2}\right\} Prob\left\{-\frac{d}{2} < n_2 < \frac{d}{2}\right\} \quad (A.9)$$

$$= (1-p)\left[1 - \left(Prob\left\{n_2 < -\frac{d}{2}\right\} + Prob\left\{n_2 > \frac{d}{2}\right\}\right)\right] \quad (A.10)$$

$$= (1-p)(1-2p) \quad (A.11)$$

The third group is the set of signals with four neighbors.

$$p_4 = Prob\left\{-\frac{d}{2} < n_1 < \frac{d}{2}\right\} Prob\left\{-\frac{d}{2} < n_2 < \frac{d}{2}\right\} \quad (A.12)$$

$$= (1-2p)^2 \quad (A.13)$$

For the 16 signal set, we have 4 signals with two neighbors, 8 signals with three neighbors, and 4 signals with four neighbors. In general for a square grid constellation, $M = 2^k$ and k is even, there are 4 signals with two neighbors, $4(\sqrt{M}-2)$ signals with three neighbors, and $(\sqrt{M}-2)^2$ signals with four neighbors. The probability of error for a symbol can then be defined as

$$P_e = 1 - \frac{1}{M}\left[4p_2 + 4(\sqrt{M}-2)p_3 + (\sqrt{M}-2)^2 p_4\right] \quad (A.14)$$

After replacing p_2, p_3, and p_4 into the above equation we obtain Eq. 2.35.

A.2.2 Derivation of p for Square Constellations

To relate P_e and the SNR, we must explicitly derive p. We refer back to the definition of p in Eq. A.6. Since this is one dimensional, we can assume for now that we have a multiamplitude signal. The received signal is expressed as,

$$r_k(t) = \alpha_k e^{-j\phi_k} A_m u(t) + z_k(t) \quad [51] \tag{A.15}$$

where

$$A_m = 2m - 1 - \sqrt{M} \quad m = 1, 2, \ldots \sqrt{M} \quad [51] \tag{A.16}$$

The following decision variable is equivalent to the output of the demodulator.

$$U_{k,m} = \Re\left\{ e^{j\phi_k} \int_0^T r_k(t) u^*(t)\, dt \right\} \tag{A.17}$$

$$= 2\alpha_k \varepsilon A_m + \nu_k \tag{A.18}$$

where

$$\nu_k = \Re\left\{ \int_0^T z_k(t) u^*(t)\, dt \right\} \tag{A.19}$$

The variance of ν_k is $2\varepsilon N_0$.

After passing through the diversity combiner the decision variable is as follows.

$$U_m = \sum_{k=1}^{L} U_{k,m} w_k \tag{A.20}$$

$$= 2\varepsilon A_m \sum_{k=1}^{L} \alpha_k w_k + \sum_{k=1}^{L} \nu_k w_k \tag{A.21}$$

U_m is a Gaussian random variable with variance of $2\varepsilon N_0 \sum_{k=1} w_k^2$.

In the absence of noise the distance between two received signals is,

$$d = 2\varepsilon(A_m - A_{m-1}) \sum_{k=1}^{L} \alpha_k w_k \quad (A.22)$$

$$= 4\varepsilon \sum_{k=1}^{L} \alpha_k w_k \quad (A.23)$$

If we replace d in Eq. A.6 with the above result and replace n with $\sum_{k=1}^{L} \nu_k w_k$, we get

$$p = Prob\left\{ \sum_{k=1}^{L} \nu_k w_k > 2\varepsilon \sum_{k=1}^{L} \alpha_k w_k \right\} \quad (A.24)$$

Since ν_k is a Gaussian random variable, we rewrite this equation in terms of a Gaussian distribution.

$$p = \frac{1}{\sqrt{2\pi\sigma_\nu^2}} \int_{2\varepsilon \sum_{k=1}^{L} \alpha_k w_k}^{\infty} e^{-x^2/2\sigma_\nu^2}\, dx \quad (A.25)$$

With the following change of variable,

$$t = \frac{x}{\sqrt{2\sigma_\nu}} \quad (A.26)$$

$$dt = \frac{dx}{\sqrt{2\sigma_\nu}} \quad (A.27)$$

we get the equation below in the form of the erfc function.

$$p = \frac{1}{\sqrt{\pi}} \int_{\frac{2\varepsilon}{\sqrt{2\sigma_\nu^2}} \sum_{k=1}^{L} \alpha_k w_k}^{\infty} e^{-t^2}\, dt \quad (A.28)$$

$$= \frac{1}{2}\mathrm{erfc}\left(\frac{\sqrt{2}\varepsilon \sum_{k=1}^{L} \alpha_k w_k}{\sigma_\nu} \right) \quad (A.29)$$

$$= \frac{1}{2}\mathrm{erfc}\left(\frac{\sqrt{2}\varepsilon \sum_{k=1}^{L} \alpha_k w_k}{\sqrt{2\varepsilon N_0 \sum_{k=1}^{L} w_k^2}} \right) \quad (A.30)$$

$$= \frac{1}{2}\mathrm{erfc}\left(\sqrt{\frac{\varepsilon \left(\sum_{k=1}^{L} \alpha_k w_k \right)^2}{N_0 \sum_{k=1}^{L} w_k^2}} \right) \quad (A.31)$$

Before proceeding any further, a notational clarification is in order. For all the previous modulation schemes, the signal energy ε was equivalent to the average signal energy ε_{AV}. So to be more precise, our definition of the average signal-to-noise ratio $\overline{\gamma_c}$ should be

$$\overline{\gamma_c} = \frac{\varepsilon_{AV}}{N_0} E[\alpha_k^2] \tag{A.32}$$

For a multiamplitude signaling scheme the signal energy is no longer equivalent to the average signal energy. Therefore we must derive ε_{AV} in terms of ε and replace ε in our equation for p. From [51], the average transmitted energy is,

$$\varepsilon_{AV} = E[A_m^2] \int_0^T |u(t)|^2 \, dt \quad [51] \tag{A.33}$$

$$= 2E[A_m^2]\varepsilon \tag{A.34}$$

The average value of A_m^2 is given in [51].

$$E[A_m^2] = \frac{M-1}{3} \tag{A.35}$$

where

$$A_m = 2m - 1 - \sqrt{M} \quad \text{for } m = 1, 2, \ldots \sqrt{M} \tag{A.36}$$

Therefore,

$$\varepsilon_{AV} = \frac{2}{3}(M-1)\varepsilon \tag{A.37}$$

And ε in terms of ε_{AV} is,

$$\varepsilon = \frac{3}{2(M-1)} \varepsilon_{AV} \tag{A.38}$$